RSC Advances

PAPER

View Article Online
View Journal | View Issue

Cite this: *RSC Adv.*, 2019, **9**, 39315

Solvothermal synthesis of Mn-doped $CsPbCl_3$ perovskite nanocrystals with tunable morphology and their size-dependent optical properties†

Chang Liu,[ab] Jing Lin,*[ab] Wei Zhai,[ab] Zhikai Wen,[ab] Xin He,[ab] Mengmeng Yu,[ab] Yang Huang,*[ab] Zhonglu Guo,[ab] Chao Yu*[ab] and Chengchun Tang[ab]

Doping metal ions in inorganic halide perovskite ($CsPbX_3$, X = Cl, Br, I) nanocrystals (NCs) endows the NCs with unique optical characteristics, and has thus attracted immense attention. However, controllable synthesis of high-quality doped perovskite NCs with tunable morphology still remains challenging. Here, we report a facile, effective and unified strategy for the controllable synthesis of Mn-doped $CsPbCl_3$ quantum dots (QDs) and nanoplatelets (NPLs) *via* a single-step solvothermal method. The incorporation of Mn^{2+} into $CsPbCl_3$ NCs introduces new broad photoluminescence (PL) emission from Mn^{2+} while maintaining the structure of host $CsPbCl_3$ NCs nearly intact. The PL intensity, emission peak position and size of the NCs can be accurately adjusted by altering the experimental parameters such as Mn-to-Pb feed ratio and reaction time. Especially, by changing the amount of ligands, Mn-doped $CsPbCl_3$ QDs, NPLs or their mixtures can be obtained. Both of the Mn-doped QDs and NPLs exhibit a size-dependent quantum confinement effect, which is confirmed by the relationship between the size of NCs and the exciton emission peaks. The solvothermal reaction condition plays an important role for the precise control of the structure, morphology and PL properties of the Mn-doped NCs. The as-prepared Mn-doped $CsPbCl_3$ NPLs with thickness down to ~2 nm exhibit a PL quantum yield (PLQY) of more than 22%. This work introduces a new strategy for the controllable synthesis of Mn-doped perovskite NCs, which provides ideas for the in-depth study of the dope-and-grow process and can be extended to approaches of doping other metal ions.

Received 11th October 2019
Accepted 15th November 2019

DOI: 10.1039/c9ra08289a

rsc.li/rsc-advances

Introduction

Inorganic lead halide perovskite ($CsPbX_3$, X = Cl, Br, I) nanocrystals (NCs) are novel semiconductor materials with prominent optical and electronic properties, relatively low cost and convenient liquid-phase synthesis process,[1–9] thus showing promising application prospects in the fields of photodetectors,[10–12] lasers,[13,14] perovskite light emitting diodes (LEDs),[15–20] X-ray detectors,[21] bio-imaging devices,[22] solar cells,[9,23–25] *etc.* Doping provides a universal and effective way to offer the semiconductor materials with new optical, electronic and magnetic properties.[26–31] For example, metal doping of II–VI semiconductor NCs (such as CdSe, ZnS) can introduce new exciton transition pathways, impart magnetism or change emission properties of the NCs.[30–33] So far, the metal doping of perovskite NCs has attracted tremendous attention and in-depth research. Various kinds of metal ions, such as Bi^{3+}, Cu^{2+}, Ni^{2+}, Mn^{2+}, Cd^{2+}, Sn^{2+}, Rb^{+} and rare earth metal ions (*e.g.*, Ce^{3+}, Eu^{3+}, Tb^{3+}) have been successfully doped into perovskite NCs.[34–53] These studies have proved that doping may endow perovskite NCs with enhanced photoluminescence (PL) quantum yields (QYs), new emission characteristics or improved stability, as compared to their undoped counterparts.

Among those selectable metal ions, the Mn^{2+} doping of $CsPbX_3$ NCs has received great interests. Theoretically, doping of Mn^{2+} into $CsPbX_3$ NCs may introduce new long-lifetime sensitized emission, where the energy transfer from the charge carriers of $CsPbX_3$ host to the d electron of Mn^{2+} resulting in the d–d transition and generation of Mn^{2+} luminescence.[42] Recently studies have shown that Mn-doped $CsPbX_3$ (X = Cl, Br, Cl/Br) quantum dots (QDs) can be successfully synthesized *via* hot injection,[39,40,47] anion exchange[46] or anti-solvent method.[44] A high Mn substitution ratio of ~46% can be obtained for Mn doped $CsPbCl_3$ QDs,[39] while the PLQYs can be greatly enhanced due to the effective energy transfer from the $CsPCl_3$ host to dopant Mn^{2+} ions.[44] However, up to now the controllable synthesis of Mn-doped perovskite NCs with precisely tuned morphology and structures still remains

[a]*School of Materials Science and Engineering, Hebei University of Technology, Tianjin 300130, P. R. China. E-mail: linjing@hebut.edu.cn; huangyang@hebut.edu.cn; yuchao20130426@126.com*

[b]*Hebei Key Laboratory of Boron Nitride Micro and Nano Materials, Hebei University of Technology, Tianjin 300130, P. R. China*

† Electronic supplementary information (ESI) available. See DOI: 10.1039/c9ra08289a

challenging. Compared with the work of obtaining QDs, there are less studies on the preparation of Mn-doped perovskite NCs with other morphology, for example, nanoplatelets (NPLs). Controllable synthesis of Mn-doped perovskite NCs with tunable morphology is of great significant for the deeply understanding of the relationship between the microstructure and PL characteristics (*i.e.* emission, excitation, PLQY, lifetime, *etc.*) of the doped perovskite NCs. Therefore, it is required to develop a new strategy for the obtaining of Mn-doped perovskite NCs with tailored morphology and opening the way for the metal-doped perovskite NCs.

Solvothermal reaction has been demonstrated to be an effective method for the controllable synthesis of $CsPbX_3$ NCs due to its mild crystal growth environment.[54] It is believed that the solvothermal method is very suitable for the preparation of Mn-doped $CsPbX_3$ NCs, since the process of NC nuclei growth and the Mn^{2+} doping would be easily controlled *via* the adjusting the solvothermal reaction times and/or temperatures. In this work, we developed a unified solvothermal method to prepare Mn-doped $CsPbCl_3$ QDs and NPLs. By reacting of the Cs-oleate and Pb/$MnCl_2$ precursors in a Teflon-lined autoclave, Mn^{2+} ions could be successfully doped into $CsPbCl_3$ NCs and new Mn^{2+} PL emission could be introduced. Because of the sealed reaction condition, there was no need to carry out a protective gas atmosphere during experiment. Interestingly, the Mn-doped $CsPbCl_3$ NCs show tunable morphology: Mn-doped QDs and NPLs can be well obtained *via* gradually changing the amount of the ligands. The relatively low solvothermal reaction temperature slows down the doping process and enables the precisely control on the emission properties, crystal structures and sizes of the Mn-doped $CsPbCl_3$ QDs and NPLs. It is noteworthy that the as-prepared ultrathin Mn-doped $CsPbCl_3$ NPLs have a thickness of down to ~2 nm, which, as far as we know, has not been achieved in other works.[55,56] The strategy provides a platform for further study on the mixing process of metal doping and crystal growth, which can be used as a reference for the property regulation of metal-doped perovskite NCs.

Experimental

Materials

Cesium carbonate (Cs_2CO_3, 99.9% metal basis) and 1-octadecene (ODE, >90%) were purchased from Macklin. Magnesium(II) chloride ($MnCl_2$, >99% trace metal basis), lead(II) chloride ($PbCl_2$, 99.99% metal basis), oleylamine (OLA, 70%) and oleic acid (OA, 90%) were obtained from Aladdin. Ethyl acetate (AR) and *n*-hexane (AR) were purchased from Beijing Chemical Reagent Ltd., China. All chemicals were employed as received with no purifications or otherwise processes.

Preparation of Cs-oleate precursor

1.995 mmol of Cs_2CO_3, 18 mL of ODE and 2.5 mL of OA were loaded into a 50 mL three-necked round-bottomed flask. The reaction mixture was then heated in an oil bath at 120 °C for 1 h, followed by raising the temperature to 150 °C and holding for 25 min until all Cs_2CO_3 reacted with OA. The Cs-oleate precursor was stored at room temperature, and a preheating process over 120 °C was necessary before use.

Preparation of Pb/$MnCl_2$ precursor

In a typical process for Mn-doped $CsPbCl_3$ QDs, 0.374 mmol of $PbCl_2$, 1.87 mmol of $MnCl_2$ and 10 mL of ODE were loaded into a 50 mL three-necked, round-bottomed flask and heated in an oil bath. When the temperature of the mixture reached 120 °C, 4 mL of OA and 4 mL of OLA were added and the temperature of the mixture was raised and kept at 130 °C until $PbCl_2$ and $MnCl_2$ were completely dissolved. Then the solution was naturally cooled down to the room temperature. For obtaining Mn-doped $CsPbCl_3$ NPLs, the reaction conditions were kept as same except the amount of OA and OLA was decreased to 2–3 mL. Generally, the preheating process was not necessary for Pb/$MnCl_2$ precursor unless precipitation occurred due to low room temperature.

Synthesis of Mn-doped $CsPbCl_3$ NCs

17 mL of Pb/$MnCl_2$ precursor and 0.8 mL of Cs-oleate precursor were loaded into a Teflon-lined autoclave and then maintained at 120 °C for different solvothermal reaction times. After that, the autoclave was naturally cooled down to the room temperature. All the experimental operations were operated in an open environment without protective gas atmosphere.

Isolation and purification

The Mn-doped $CsPbCl_3$ NCs were extracted and separated from the crude solution by centrifugation at 8500 rpm for 5 min. The supernatant was then discarded and meanwhile 5 mL of *n*-hexene was used to redispersed the precipitates. Thereafter, 5 mL of ethyl acetate was added to induce aggregation and remove excess ligands, followed by another centrifugation at 8500 rpm for 5 min. After that, the precipitates were dispersed in 10 mL of *n*-hexane to form a long-term stable colloidal solution. For obtaining more uniform colloidal solution, centrifugation at 3500 rpm for 5 min is necessary to remove relatively large nanoparticles.

Characterization

The UV-visible spectrophotometry (UV-vis) measurements were collected on a Japan HITACHI U-3900H spectrometer. Transmission electron microscopy (TEM) and Energy-Dispersive X-ray (EDX) spectroscopy measurements were collected on a Philips Tecnai F20 microscope at an accelerate voltage of 200 kV. Powder X-ray diffraction patterns (XRD) were measured on a Bruker D8 Advance diffractometer using Cu Kα radiation (λ = 1.5406 Å). For the preparation of XRD samples, 1–2 mL of as-prepared colloidal solution are dripped onto a zero-diffraction silicon wafer. The PL spectra and PLQY measurements were acquired using a Fluorolog-3 Horiba Jobin-Yvon spectrofluorimeter (excited at 365 nm) equipped with an integrating sphere. PL lifetimes were measured using a time-corrected single-photon-counting (TCSPC) system. The wavelengths of

the excitation sources for exciton emission peak and Mn^{2+} emission peak are 371 nm (by a pulsed diode light source) and 365 nm (by a Xenon lamp), respectively.

Results and discussion

In this work, the Mn-doped $CsPbCl_3$ NCs were prepared *via* a facile solvothermal method in which Mn was introduced into Pb precursors by simply adding of additional $MnCl_2$. Both of QDs and NPLs can be well prepared *via* changing the amount of OA and OLA in the precursor.

Synthesis and properties of Mn-doped $CsPbCl_3$ QDs

Firstly, Mn-doped $CsPbCl_3$ QDs with low doping concentration were prepared with a Mn-to-Pb molar feed ratio of 5 : 1 and a low solvothermal treatment temperature of 120 °C. The typical TEM image (Fig. 1a) shows that the QDs have uniform cube morphology with an average size of ~8.2 nm. EDX analysis reveals the composition of QDs as $CsPb_{0.94}Mn_{0.06}Cl_3$ (Fig. S1†). High-resolution TEM (HRTEM) image (Fig. 1b) indicates the single crystal structure and good crystallization of the QDs. The crystal lattices are observed with the interplanar distances of ~3.98 and ~2.86 Å, which can be assigned to the (101) and (200) planes of tetragonal $CsPbCl_3$, respectively. XRD pattern confirms that the as-prepared QDs have crystalline structure of tetragonal $CsPbCl_3$ (PDF card no. 18-366), which also indicates that the lightly doping of Mn^{2+} doesn't change the initial structure of perovskite. Moreover, as compared to pure tetragonal $CsPbCl_3$, a slight peak shift has been observed, which can be attributed to the incorporation of Mn^{2+} in $CsPbCl_3$. The Mn^{2+} ions (97 pm, crystal radius) are likely to occupy the position of the isovalent but larger Pb^{2+} ions (133 pm, crystal radius) and cause the lattice distortion.[45]

Then we studied the optical properties of the as-prepared QDs. The PL excitation (PLE), UV-vis absorption and PL emission spectra are shown in Fig. 1d–e. The UV-vis spectrum (Fig. 1d) shows that the as-prepared QDs have a noticeably strong first exciton absorption peak of 377 nm, which is blue-shifted and exhibits the feature of quantum confinement effect, as compared to the bulk $CsPbCl_3$.[57] Under the excitation of UV light at 365 nm, dual emission peaks are observed in PL emission spectrum, which are located at 403 nm and 572 nm, respectively. The peak at 403 nm is attributed to the inherent exciton emission of $CsPbCl_3$ QDs and shows a narrow FWHM (full width at half maximum) of 14 nm. The as-prepared QDs reveals a noticeable Stokes shift of 26 nm, which is larger than that obtained in previous reports.[39,45] The larger Stokes shift reduces the self-absorption of QDs, which is benefit to their optical properties. Additional weak peak at 572 nm arises from the incorporation of Mn^{2+} and displays a relatively broad FWHM of ~56 nm. The excitation spectra of dual peaks were also tested and shown in Fig. 1e. The excitation spectra of the exciton emission (403 nm) and Mn^{2+} emission (572 nm) both perform almost coincident curves with the absorption spectrum, which can be explained by the effective energy transfer from the $CsPbCl_3$ host to dopant Mn^{2+} ions.[44,58]

To further investigate the mechanism of dual emission, the PL lifetimes of Mn-doped $CsPbCl_3$ QDs were measured and shown in Fig. 1f and g, respectively. The dual emission peaks of the QDs have completely different PL lifetimes: the average PL lifetime of exciton emission peak (403 nm) is 2.32 ns, while the average PL lifetime of Mn^{2+} emission peak (572 nm) is 1.73 ms. The exciton lifetime originates from the $CsPbCl_3$ host, which can be well fitted to two-exponential decay with a long lifetime component of 6.02 ns and a short lifetime component of 0.58 ns. As has been reported, the PL emission of $CsPbCl_3$ derives from the radiative recombination (generated by the relaxation of excitons) and non-radiative recombination (generated by electronic traps or surface defects),[14,59] corresponding to the long lifetime and short lifetime, respectively. Differently, the Mn^{2+} luminescence lifetime decay curve displays a noticeable single-exponential decay and an extremely long relaxation time,

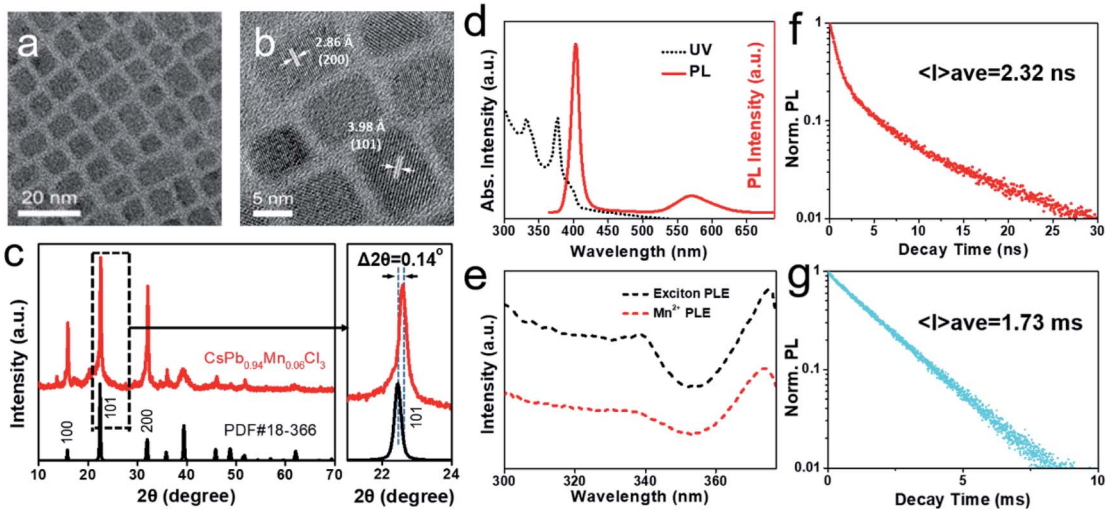

Fig. 1 (a) TEM image, (b) HRTEM image, (c) XRD pattern, (d) UV-vis absorption and PL emission spectra, (e) PLE spectra, (f) exciton PL lifetime and (g) Mn^{2+} luminescence lifetime of a typical Mn-doped $CsPbCl_3$ QDs (prepared using Mn-to-Pb molar feed ratio of 5 : 1 and reacting at 120 °C for 3 h).

which is related to its unique luminescence mechanism. By combining the spectral analysis with previous report on the luminescence of Mn^{2+} doped semiconductors, the Mn^{2+} luminescence mechanism can be explained briefly as follows: the incorporation of Mn^{2+} provides a new energy transfer pathway from the excited $CsPbCl_3$ host to d electrons of Mn^{2+}, which enhances the internal d–d transition ($^4T_1$ to $^6A_1$) of Mn^{2+} and generates new emission channel.[42,60,61]

To reveal the effect of solvothermal reaction times on the PL properties of $CsPbCl_3$ QDs with low Mn doping ratio, we prolonged the reaction time to obtained a series of samples. As shown in Fig. S2a and Table S1,† the QDs obtained after 3, 6, 9 h display similar PL emission and their PL quantum yields (PLQYs) remains in the range of 4.8–6%. Their PL decay curves (Fig. S2b, c, Tables S1 and S2†) also display a negligible change. We believe that the earlier arrival of reaction equilibrium results in low doping ratio of Mn^{2+}. Moreover, with the increase of reaction time, the Mn^{2+} doping ratio and the surface defects of the QDs did not increased notably, resulting in no significant changes in PLQYs and lifetimes. Therefore, the prolonged reaction time contributes little to increasing the doping ratio of Mn^{2+} into $CsPbCl_3$ QDs.

The low Mn^{2+} doping ratio of the QDs suggests lower thermodynamics reactivity of Mn^{2+} ions as compared to Pb^{2+} ions during the solvothermal reaction. In order to efficiently increase the doping ratio, higher Mn-to-Pb feed ratios were employed during the preparation of $Pb/MnCl_2$ precursor. Here, we increased the Mn-to-Pb feed ratio from 5 : 1 to 7.5 : 1 and 10 : 1 and fixed the other reaction conditions (120 °C for 3 h) to obtain Mn-doped $CsPbCl_3$ QDs with different doping ratios. EDX measurement reveals the compositions of the QDs as $CsPb_{0.94}Mn_{0.06}Cl_3$, $CsPb_{0.85}Mn_{0.15}Cl_3$ and $CsPb_{0.75}Mn_{0.25}Cl_3$ (Fig. S1†), respectively. XRD patterns (Fig. 2a) exhibit a continuous peak shift as the doping ratio increases. A 0.12° shift to a higher angle of (101) plane can be observed, which indicates that the increase in incorporation of Mn^{2+} aggravates the lattice contraction. In addition, the peaks of hexagonal $CsMnCl_3$ (PDF card no. 25-219) and rhombohedral (*i.e.*, trigonal) $CsMnCl_3$ (PDF card no. 73-227) gradually appear, indicating that a relatively high doping ratio may lead Pb^{2+} ions sites completely replaced by Mn^{2+} ions in partial areas. After excess ions replacement, the crystalline structure of the $CsPbCl_3$ host is destroyed and new phases of $CsMnCl_3$ are formed by a spinodal decomposition process.[56] The newly generated $CsMnCl_3$ NCs exhibit hexagon morphology with relatively larger size of 16–32 nm (Fig. S3†). In fact, the sample prepared after a prolonged reaction time over 12 h exhibits the phase composition of almost h-$CsMnCl_3$ and r-$CsMnCl_3$ (Fig. S4†). In addition, an extra peak located at ~25.5° is noticed in the XRD pattern (black triangle in Fig. 2a), which has also been observed in other related works.[56] The existence of the extra peak may indicate that at a relatively high doping ratio, Mn^{2+} ions not only replace the position pf Pb^{2+} ions, but also have other forms of incorporation, such as occupying the space in the lattice of $CsPbCl_3$ host.[39] PL emission spectra (Fig. 2b) of the samples show that as the doping ratio increases, the intensity of the broad Mn^{2+} emission peak increases significantly, which is attributed to the enhancement in the energy transfer from excitons to Mn^{2+}. The $CsPb_{0.75}Mn_{0.25}Cl_3$ sample shows bright yellow-orange colored emission (Fig. S5†) with a PLQY of over 30%. As doping ratio increases, the exciton emission shows a blue shift, which is related to the size-dependent quantum confinement effect of the QDs. As is shown in the TEM images (Fig. 2c–e), the size of the QDs decreases from 8.2 nm, 6.6 nm to 5 nm.

Synthesis and properties of Mn-doped $CsPbCl_3$ NPLs

The morphology of the product can be tuned by changing the amount of organic ligands (OA and OLA). Fig. 3a shows a typical TEM image of the sample obtained by using 2 mL of OA and 2 mL of OLA, while the Mn-to-Pb molar feed ratio was kept at 5 : 1. The as-prepared sample exhibits uniform platelet morphology. The observed square or thin rectangle shapes are consistent to the NPLs lying parallel or perpendicular to the carbon film, respectively. The NPLs have an average lateral

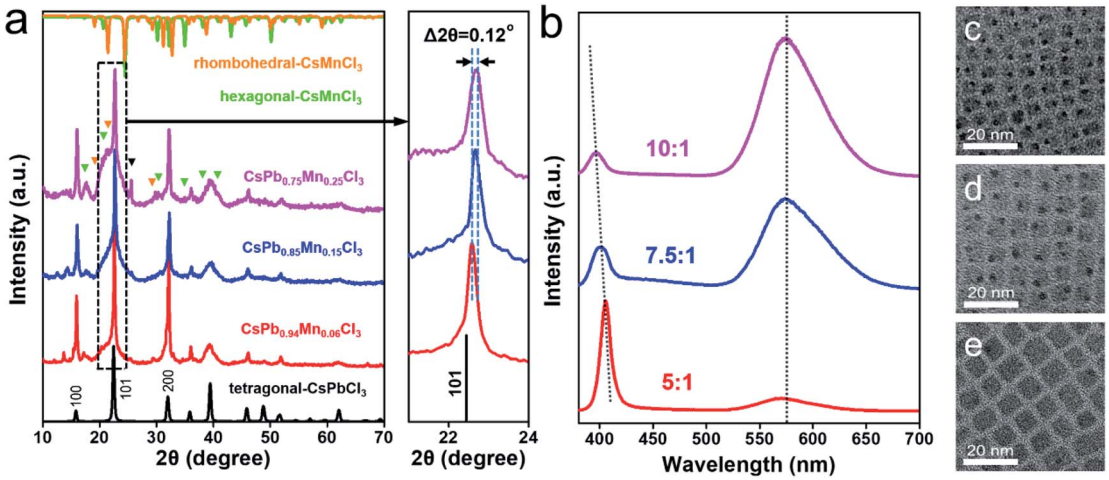

Fig. 2 (a) XRD patterns of Mn-doped $CsPbCl_3$ QDs prepared with Mn-to-Pb molar feed ratios of 10 : 1, 7.5 : 1 and 5 : 1, respectively. (Right) Magnified peak shifts of (101) plane. (b) PL emission spectra of the QDs. (c–e) TEM images of Mn-doped $CsPbCl_3$ QDs prepared with different Mn-to-Pb molar feed ratios: 10 : 1 (c), 7.5 : 1 (d) and 5 : 1 (e).

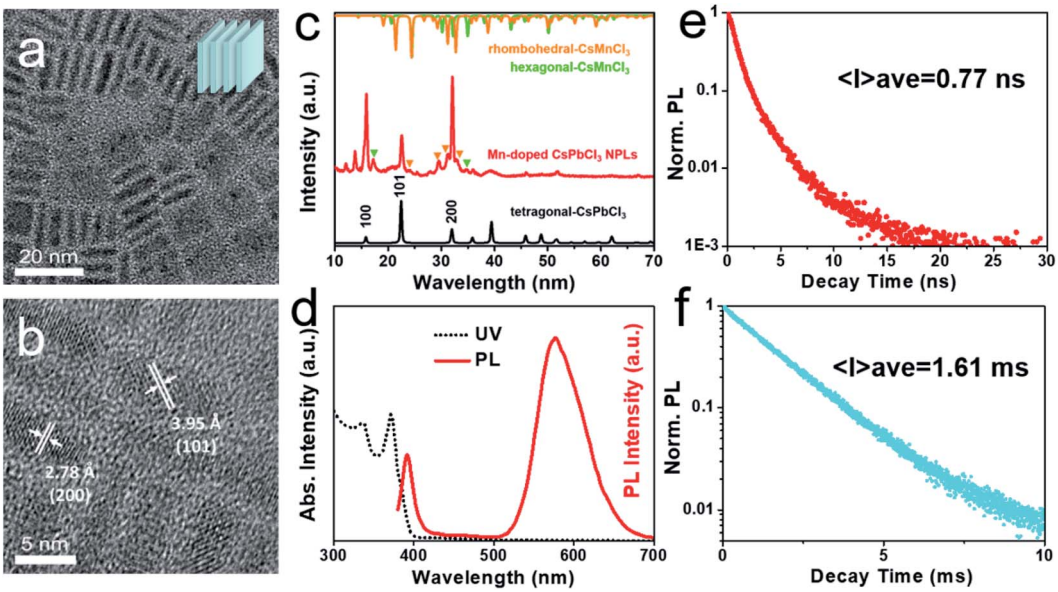

Fig. 3 (a) TEM image, (b) HRTEM image, and (c) XRD pattern of typical Mn-doped $CsPbCl_3$ NPLs (using Mn-to-Pb molar feed ratio of 5 : 1 and reacting for 4.5 h). (d) UV-vis absorption and PL emission spectra, (e) exciton PL lifetime and (f) Mn^{2+} luminescence lifetime spectrum of the Mn-doped $CsPbCl_3$ NPLs.

length of ~11 nm and an average thickness of ~2.3 nm. EDX measurement exposes the NPLs with a composition of $CsPb_{0.65}Mn_{0.35}Cl_3$ (Fig. S6†). As compared with the as-prepared $CsPb_{0.94}Mn_{0.06}Cl_3$ QDs, the NPLs show a much higher Mn doping concentration (~35%), suggesting that less amount of ligands contributes to the incorporation of Mn^{2+}. High-resolution TEM (HRTEM) image (Fig. 3b) suggests the good crystallinity of NPLs with clearly lattice fringes. The distances between lattice planes of 3.95 Å and 2.78 Å correspond to the (101) and (200) planes of tetragonal $CsPbCl_3$, respectively, which are smaller than that of Mn-doped $CsPbCl_3$ QDs, indicating more incorporation of Mn^{2+}. XRD result (Fig. 3c) reveals the main crystal structure of tetragonal $CsPbCl_3$, and the appearance of $CsMnCl_3$ phase in the product, similar as that of Mn-doped QDs.

The UV-vis and PL spectra of Mn-doped $CsPbCl_3$ NPLs (Fig. 3d) display an absorption peak at 371 nm and an exciton emission peak at 392 nm, which are both blue-shifted as compared to that of Mn-doped $CsPbCl_3$ QDs. The blue shift originates from the ultra-small thickness of NPLs, suggesting their size-dependent quantum confinement effect. The Mn^{2+} emission peak centered at 577 nm is red-shifted compared to that of Mn-doped $CsPbCl_3$ QDs (572 nm), proving stronger Mn–Mn interaction and contributing an orange colored emission.[57] The PL decay curves (Fig. 3e and f) of the NPLs also reveal two different lifetimes. The average PL lifetimes of exciton emission and the Mn^{2+} emission are 0.77 ns and 1.61 ms, respectively. As compared with Mn-doped QDs, the exciton lifetime exhibits similar two-exponential fitting curve, but the lifetime is much shorter than that of QDs (2.32 ns), which mainly related to a higher incorporation of Mn^{2+} and stronger energy transfer from $CsPbCl_3$ to Mn^{2+}. The Mn^{2+} luminescence lifetime curve can be better fitted to two-exponential decays than single-exponential decay, indicating that the formation of new $CsMnCl_3$ phase causes heterogeneous environment around Mn^{2+} ions.[56]

We further studied the effects of solvothermal reaction times on the optical properties of Mn-doped $CsPbCl_3$ NPLs. PL emission spectra (Fig. 4a) show that as the reaction time increases, the exciton emission peak shifts from 389 nm to 398 nm, which is attributed to size-dependent quantum confinement effect. Thus, we can easily and precisely control the optical properties of Mn-doped $CsPbCl_3$ NPLs *via* changing the reaction times. As the reaction time increases, the surface defects decreased, resulting in stronger emission of the $CsPbCl_3$ host and the energy transfer to Mn^{2+}. Directly seen from the results, the prolonged reaction time yields an increase in the intensities of dual emission peaks and an increase of PLQY (Fig. 4b) from 10.4% to 22.2%. The HRTEM images of NPLs obtained for different reaction times are shown in Fig. 4c–f. The average thickness of NPLs can be accurately acquired by measuring those stacked perpendicular NPLs. With the reaction time increasing, the thickness of the NPLs changes from 2.21 ± 0.41 nm, to 2.96 ± 0.56 nm (Fig. 4h–k), exhibiting a positive correlation with the shift of exciton emission peak, as shown in Fig. 4g. The result indicates that the thickness and the emission peak position of the NPLs can be tuned precisely by the solvothermal reaction time.

Tunable morphology and optical properties of Mn-doped $CsPbCl_3$ NCs

By carrying out synthesis processes with different amounts of organic ligands (OA and OLA), Mn-doped $CsPbCl_3$ QDs and NPLs were successfully obtained. Then we gradually changed the amount of ligands for further investigation of ligand-dependent morphology of Mn-doped perovskite NCs. As

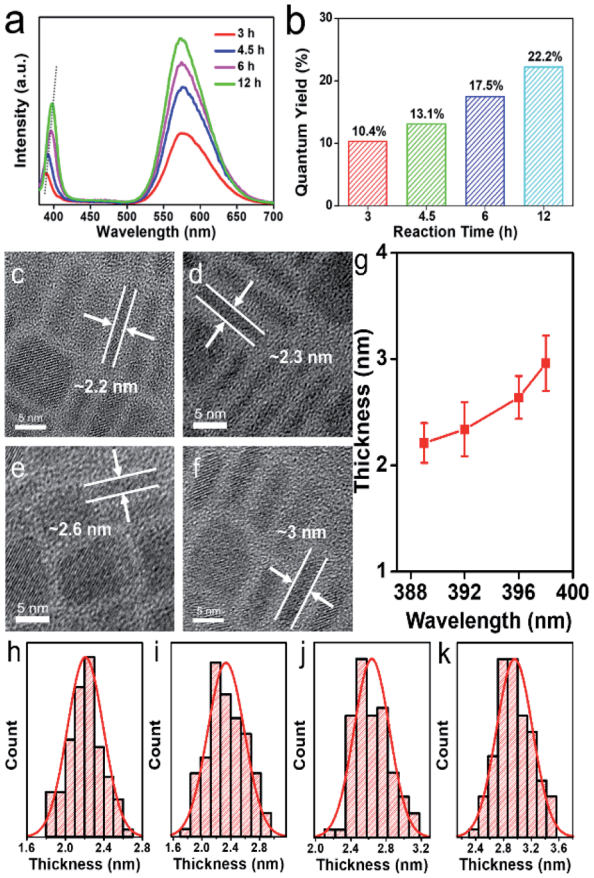

Fig. 4 (a) PL emission spectra and (b) PLQYs of Mn-doped $CsPbCl_3$ NPLs prepared under different reaction times. (c–f) HRTEM images of different NPLs prepared under 3 h (c), 4.5 h (d), 6 h (e) and 12 h (f). (g) Thickness as a function of the exciton emission peak wavelength. (h–k) The corresponding thickness histograms of Mn-doped $CsPbCl_3$ NPLs samples.

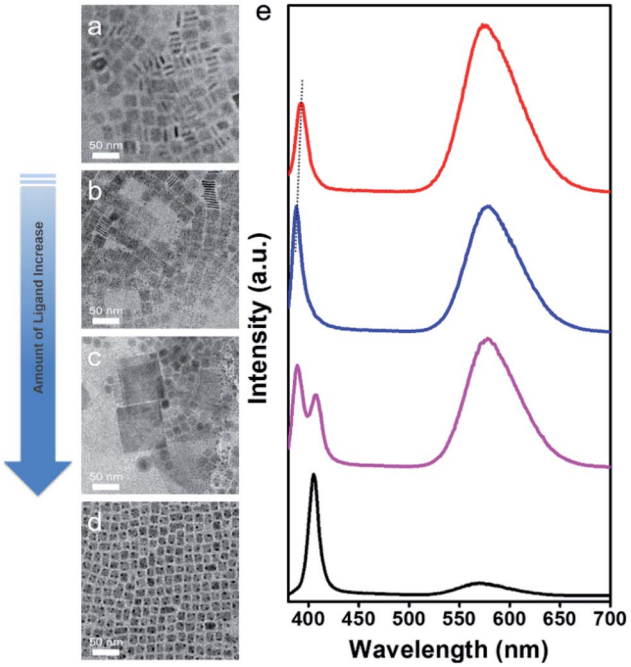

Fig. 5 (a–d) Low magnification TEM images of Mn-doped $CsPbCl_3$ NCs prepared as a function of the amount of ligand. (e) The corresponding PL emission spectra of Mn-doped $CsPbCl_3$ NCs.

revealed in Fig. 5a–d, the morphology changes from NPLs to QDs as the amount of ligands increases. Large amount of NPLs with a lateral size of ~10 nm and a thickness of ~2.2 nm (Fig. 5a, also shown in Fig. 4c) are obtained when 2 mL of OA and OLA were used. As the amount of ligand increases (3 mL of OA and OLA), ultrathin NPLs with a lateral size of ~20 nm and a thickness of only ~2 nm (Fig. 5b and S7†) are formed. To the best of our knowledge, the synthesis of ultrathin Mn-doped $CsPbCl_3$ NPLs with a thickness of only ~2 nm is challenging, which were not achieved in other works. When the amount of ligands continues to increase (3.5 mL of OA and OLA), a mixed morphology of NPLs and QDs are obtained (Fig. 5c), in which the NPLs grow larger with lateral sizes of 50–100 nm. Finally, when using 4 mL of OA and OLA, only QDs with average size of ~8.2 nm (Fig. 5d) can be achieved. Typical PL spectra for different samples are shown in Fig. 5e. The exciton emission peaks are determined by the morphology and sizes of the NCs due to the quantum confinement effect, which is consistent with the previous discussion. The broad Mn^{2+} emission derives from the energy transfer from $CsPbCl_3$ host to Mn^{2+}. Under the same Mn-to-Pb feed ratio, Mn^{2+} is more likely to be doped into $CsPbCl_3$ NPLs than that of $CsPbCl_3$ QDs, leading to stronger intensity of Mn^{2+} emission peak.

As we know, the organic ligands (OA and OLA) coordinate with ions and assume the function of slowing and controlling the growth of perovskite NCs.[62] Due to the anisotropy of the perovskite NCs, changes in the amount of ligands give rise to different crystal growth orientation. When the amount of ligands is relatively small, two-dimensional NPLs morphology is more likely to be obtained in a relatively slow solvothermal reaction condition owing to the differential binding effect of capping ligands in different directions of the NCs. When the amount of the ligands increases, the binding effect on the NCs in different directions tends to be uniform, thereby forming morphology of QDs (nanocubes). Furthermore, because of the relatively low reactivity of Mn^{2+} ions, the doping process is followed by the formation of $CsPbCl_3$ NCs. Thus, we believe that more capping ligands prevent $CsPbCl_3$ NCs from effective incorporation of Mn^{2+}, resulting in a lower Mn^{2+} concentration in $CsPbCl_3$ QDs as compared to that of NPLs prepared under the same reaction parameters.

Conclusions

In summary, we develop a facile and effective single-step solvothermal method on controllable synthesis of Mn-doped $CsPbCl_3$ NCs. By altering the amount of ligands, Mn-doped $CsPbCl_3$ with morphology of QDs or NPLs can be well obtained respectively. The doping of Mn^{2+} introduces an energy transfer pathway from $CsPbCl_3$ host to dopant, which leads to

d–d transitions ($^4T_1$ to $^6A_1$) of the Mn^{2+} and generates Mn^{2+} luminescence. The relatively low reactivity of Mn^{2+} results in the maintaining of tetragonal $CsPbCl_3$ crystal structure. The PL intensity, emission peak position and size of the doped QDs and NPLs can be precisely controlled by varying the experimental parameters such as Mn-to-Pb feed ratio and reaction time. Both of the Mn-doped NCs exhibit strong size-dependent quantum confinement effect since the size of QDs and the thickness of NPLs are within the quantum confinement regime. The thinnest thickness of as-prepared Mn-doped $CsPbCl_3$ NPLs reaches ~2 nm, which is challenging in Mn-doped NPLs. The ultrathin two-dimensional structure and good crystallinity of Mn-doped $CsPbCl_3$ NPLs suggest an excellent application adaptability. The unified solvothermal method provides not only a new approach for the controllable preparation of Mn-doped QDs and NPLs but also new ideas for the investigation of the dope-and-grow process, which can be extended to morphology-controlling engineering of perovskite with different metal dopant and halide composition.

Conflicts of interest

There are no conflicts to declare.

Acknowledgements

This work was supported by the National Natural Science Foundation of China (51972096, 51772075, 51572068, 21806029), the Natural Science Foundation of Hebei Province (E2019202086, E2019202347), and the Program for Changjiang Scholars and Innovative Research Team in University (PCSIRT: IRT17R33).

Notes and references

1 L. Protesescu, S. Yakunin, M. I. Bodnarchuk, F. Krieg, R. Caputo, C. H. Hendon, R. X. Yang, A. Walsh and M. V. Kovalenko, *Nano Lett.*, 2015, **15**, 3692–3696.
2 X. J. Zhang, H. C. Wang, A. C. Tang, S. Y. Lin, H. C. Tong, C. Y. Chen, Y. C. Lee, T. L. Tsai and R. S. Liu, *Chem. Mater.*, 2016, **28**, 8493–8497.
3 J. De Roo, M. Ibanez, P. Geiregat, G. Nedelcu, W. Walravens, J. Maes, J. C. Martins, I. Van Driessche, M. V. Koyalenko and Z. Hens, *ACS Nano*, 2016, **10**, 2071–2081.
4 Y. S. Park, S. J. Guo, N. S. Makarov and V. I. Klimov, *ACS Nano*, 2015, **9**, 10386–10393.
5 S. Sun, D. Yuan, Y. Xu, A. Wang and Z. Deng, *ACS Nano*, 2016, **10**, 3648–3657.
6 Z. J. Li, E. Hofman, A. H. Davis, M. M. Maye and W. Zheng, *Chem. Mater.*, 2018, **30**, 3854–3860.
7 X. Chen, L. Peng, K. Huang, Z. Shi, R. Xie and W. Yang, *Nano Res.*, 2016, **9**, 1994–2006.
8 D. Yang, Y. Zou, P. Li, Q. Liu, L. Wu, H. Hu, Y. Xu, B. Sun, Q. Zhang and S. T. Lee, *Nano Energy*, 2018, **47**, 235–242.
9 A. Swarnkar, A. R. Marshall, E. M. Sanehira, B. D. Chernomordik, D. T. Moore, J. A. Christians, T. Chakrabarti and J. M. Luther, *Science*, 2016, **354**, 92–95.
10 P. Ramasamy, D. H. Lim, B. Kim, S. H. Lee, M. S. Lee and J. S. Lee, *Chem. Commun.*, 2016, **52**, 2067–2070.
11 A. Waleed, M. M. Tavakoli, L. L. Gu, S. Hussain, D. Q. Zhang, S. Poddar, Z. Y. Wang, R. J. Zhang and Z. Y. Fan, *Nano Lett.*, 2017, **17**, 4951–4957.
12 W. Zhai, J. Lin, C. Li, S. M. Hu, Y. Huang, C. Yu, Z. K. Wen, Z. Y. Liu, Y. Fang and C. C. Tang, *Nanoscale*, 2018, **10**, 21451–21458.
13 J. Butkus, P. Vashishtha, K. Chen, J. K. Gallaher, S. K. K. Prasad, D. Z. Metin, G. Laufersky, N. Gaston, J. E. Halpert and J. M. Hodgkiss, *Chem. Mater.*, 2017, **29**, 3644–3652.
14 F. Liu, Y. Zhang, C. Ding, S. Kobayashi, T. Izuishi, N. Nakazawa, T. Toyoda, T. Ohta, S. Hayase, T. Minemoto, K. Yoshino, S. Dai and Q. Shen, *ACS Nano*, 2017, **11**, 10373–10383.
15 J. Pan, L. N. Quan, Y. Zhao, W. Peng, B. Murali, S. P. Sarmah, M. Yuan, L. Sinatra, N. M. Alyami and J. J. A. M. Liu, *Adv. Mater.*, 2016, **28**, 8718–8725.
16 J. Song, J. Li, X. Li, L. Xu, Y. Dong and H. Zeng, *Adv. Mater.*, 2015, **27**, 7162–7167.
17 X. Li, Y. Wu, S. Zhang, B. Cai, Y. Gu, J. Song and H. Zeng, *Adv. Funct. Mater.*, 2016, **26**, 2435–2445.
18 M. Chen, Y. Zou, L. Wu, Q. Pan, D. Yang, H. Hu, Y. Tan, Q. Zhong, Y. Xu, H. Liu, B. Sun and Q. Zhang, *Adv. Funct. Mater.*, 2017, **27**, 1701121.
19 J. Pan, Y. Q. Shang, J. Yin, M. De Bastiani, W. Peng, I. Dursun, L. Sinatra, A. M. El-Zohry, M. N. Hedhili, A. H. Emwas, O. F. Mohammed, Z. J. Ning and O. M. Bakr, *J. Am. Chem. Soc.*, 2018, **140**, 562–565.
20 B. Jeong, H. Han, Y. J. Choi, S. H. Cho, E. H. Kim, S. W. Lee, J. S. Kim, C. Park, D. Kim and C. Park, *Adv. Funct. Mater.*, 2018, **28**, 1706401.
21 C. X. Bao, Z. L. Chen, Y. J. Fang, H. T. Wei, Y. H. Deng, X. Xiao, L. L. Li and J. S. Huang, *Adv. Mater.*, 2017, **29**, 1703209.
22 Y. W. Wang, Y. H. Zhu, J. F. Huang, J. Cai, J. R. Zhu, X. L. Yang, J. H. Shen, H. Jiang and C. Z. Li, *J. Phys. Chem. Lett.*, 2016, **7**, 4253–4258.
23 N. G. Park, M. Gratzel, T. Miyasaka, K. Zhu and K. Emery, *Nat. Energy*, 2016, **1**, 16152.
24 Q. A. Akkerman, M. Gandini, F. Di Stasio, P. Rastogi, F. Palazon, G. Bertoni, J. M. Ball, M. Prato, A. Petrozza and L. Manna, *Nat. Energy*, 2017, **2**, 16194.
25 Z. L. Chen, Q. F. Dong, Y. Liu, C. X. Bao, Y. J. Fang, Y. Lin, S. Tang, Q. Wang, X. Xiao, Y. Bai, Y. H. Deng and J. S. Huang, *Nat. Commun.*, 2017, **8**, 1890.
26 V. A. Vlaskin, C. J. Barrows, C. S. Erickson and D. R. Gamelin, *J. Am. Chem. Soc.*, 2013, **135**, 14380–14389.
27 D. Mocatta, G. Cohen, J. Schattner, O. Millo, E. Rabani and U. Banin, *Science*, 2011, **332**, 77–81.
28 Z. J. Li, E. Hofman, A. Blaker, A. H. Davis, B. Dzikovski, D. K. Ma and W. Zheng, *ACS Nano*, 2017, **11**, 12591–12600.
29 W. Zheng, K. Singh, Z. Wang, J. T. Wright, J. van Tol, N. S. Dalal, R. W. Meulenberg and G. F. Strouse, *J. Am. Chem. Soc.*, 2012, **134**, 5577–5585.

30 N. Pradhan and X. G. Peng, *J. Am. Chem. Soc.*, 2007, **129**, 3339–3347.
31 A. Sahu, M. S. Kang, A. Kompch, C. Notthoff, A. W. Wills, D. Deng, M. Winterer, C. D. Frisbie and D. J. Norris, *Nano Lett.*, 2012, **12**, 2587–2594.
32 W. W. Zheng and G. F. Strouse, *J. Am. Chem. Soc.*, 2011, **133**, 7482–7489.
33 J. H. Yu, X. Y. Liu, K. E. Kweon, J. Joo, J. Park, K. T. Ko, D. Lee, S. P. Shen, K. Tivakornsasithorn, J. S. Son, J. H. Park, Y. W. Kim, G. S. Hwang, M. Dobrowolska, J. K. Furdyna and T. Hyeon, *Nat. Mater.*, 2010, **9**, 47–53.
34 F. P. Zhu, Z. J. Yong, B. M. Liu, Y. M. Chen, Y. Zhou, J. P. Ma, H. T. Sun and Y. Z. Fang, *Opt. Express*, 2017, **25**, 33283–33289.
35 R. Begum, M. R. Parida, A. L. Abdelhady, B. Murali, N. M. Alyami, G. H. Ahmed, M. N. Hedhili, O. M. Bakr and O. F. Mohammed, *J. Am. Chem. Soc.*, 2017, **139**, 731–737.
36 C. H. Bi, S. X. Wang, Q. Li, S. V. Kershaw, J. J. Tian and A. L. Rogach, *J. Phys. Chem. Lett.*, 2019, **10**, 943–952.
37 Z. J. Yong, S. Q. Guo, J. P. Ma, J. Y. Zhang, Z. Y. Li, Y. M. Chen, B. B. Zhang, Y. Zhou, J. Shu, J. L. Gu, L. R. Zheng, O. M. Bakr and H. T. Sun, *J. Am. Chem. Soc.*, 2018, **140**, 9942–9951.
38 S. Das Adhikari, S. K. Dutta, A. Dutta, A. K. Guria and N. Pradhan, *Angew. Chem., Int. Ed.*, 2017, **56**, 8746–8750.
39 H. Liu, Z. Wu, J. Shao, D. Yao, H. Gao, Y. Liu, W. Yu, H. Zhang and B. Yang, *ACS Nano*, 2017, **11**, 2239–2247.
40 D. Parobek, Y. Dong, T. Qiao and D. H. Son, *Chem. Mater.*, 2018, **30**, 2939–2944.
41 K. Xu and A. Meijerink, *Chem. Mater.*, 2018, **30**, 5346–5352.
42 D. Parobek, B. J. Roman, Y. Dong, H. Jin, E. Lee, M. Sheldon and D. H. Son, *Nano Lett.*, 2016, **16**, 7376–7380.
43 K. Xu, C. C. Lin, X. Xie and A. Meijerink, *Chem. Mater.*, 2017, **29**, 4265–4272.
44 J. Zhu, X. Yang, Y. Zhu, Y. Wang, J. Cai, J. Shen, L. Sun and C. Li, *J. Phys. Chem. Lett.*, 2017, **8**, 4167–4171.
45 W. Liu, Q. Lin, H. Li, K. Wu, I. Robel, J. M. Pietryga and V. I. Klimov, *J. Am. Chem. Soc.*, 2016, **138**, 14954–14961.
46 G. G. Huang, C. L. Wang, S. H. Xu, S. F. Zong, J. Lu, Z. Y. Wang, C. G. Lu and Y. P. Cui, *Adv. Mater.*, 2017, **29**, 1700095.
47 X. Yuan, S. H. Ji, M. C. De Siena, L. L. Fei, Z. Zhao, Y. J. Wang, H. B. Li, J. L. Zhao and D. R. Gamelin, *Chem. Mater.*, 2017, **29**, 8003–8011.
48 W. van der Stam, J. J. Geuchies, T. Altantzis, K. H. W. van den Bos, J. D. Meeldijk, S. Van Aert, S. Bals, D. Vanmaekelbergh and C. D. Donega, *J. Am. Chem. Soc.*, 2017, **139**, 4087–4097.
49 T. Lei, M. L. Lai, Q. Kong, D. Y. Lu, W. Lee, L. T. Dou, V. Wu, Y. Yu and P. D. Yang, *Nano Lett.*, 2018, **18**, 3538–3542.
50 M. Saliba, T. Matsui, K. Domanski, J. Y. Seo, A. Ummadisingu, S. M. Zakeeruddin, J. P. Correa-Baena, W. R. Tress, A. Abate, A. Hagfeldt and M. Gratzel, *Science*, 2016, **354**, 206–209.
51 G. C. Pan, X. Bai, D. W. Yang, X. Chen, P. T. Jing, S. N. Qu, L. J. Zhang, D. L. Zhou, J. Y. Zhu, W. Xu, B. Dong and H. W. Song, *Nano Lett.*, 2017, **17**, 8005–8011.
52 Q. S. Hu, Z. Li, Z. F. Tan, H. B. Song, C. Ge, G. D. Niu, J. T. Han and J. Tang, *Adv. Opt. Mater.*, 2018, **6**, 1700864.
53 J. S. Yao, J. Ge, B. N. Han, K. H. Wang, H. B. Yao, H. L. Yu, J. H. Li, B. S. Zhu, J. Z. Song, C. Chen, Q. Zhang, H. B. Zeng, Y. Luo and S. H. Yu, *J. Am. Chem. Soc.*, 2018, **140**, 3626–3634.
54 W. Zhai, J. Lin, Q. L. Li, K. Zheng, Y. Huang, Y. Z. Yao, X. He, L. L. Li, C. Yu, C. Liu, Y. Fang, Z. Y. Liu and C. C. Tang, *Chem. Mater.*, 2018, **30**, 3714–3721.
55 W. J. Mir, M. Jagadeeswararao, S. Das and A. Nag, *ACS Energy Lett.*, 2017, **2**, 537–543.
56 Z. J. Li, E. Hofman, A. H. Davis, A. Khammang, J. T. Wright, B. Dzikovski, R. W. Meulenberg and W. Zheng, *Chem. Mater.*, 2018, **30**, 6400–6409.
57 D. D. Zhang, S. W. Eaton, Y. Yu, L. T. Dou and P. D. Yang, *J. Am. Chem. Soc.*, 2015, **137**, 9230–9233.
58 E. Hofman, R. J. Robinson, Z. J. Li, B. Dzikovski and W. W. Zheng, *J. Am. Chem. Soc.*, 2017, **139**, 8878–8885.
59 K. F. Wu, G. J. Liang, Q. Y. Shane, Y. P. Ren, D. G. Kong and T. Q. Lian, *J. Am. Chem. Soc.*, 2015, **137**, 12792–12795.
60 S. Mahamuni, A. D. Lad and S. Patole, *J. Phys. Chem. C*, 2008, **112**, 2271–2277.
61 D. J. Norris, N. Yao, F. T. Charnock and T. A. Kennedy, *Nano Lett.*, 2001, **1**, 3–7.
62 A. Z. Pan, B. He, X. Y. Fan, Z. K. Liu, J. J. Urban, A. P. Alivisatos, L. He and Y. Liu, *ACS Nano*, 2016, **10**, 7943–7954.